Check for updates

Received: 18 March 2022 | Revised: 29 June 2022 | Accepted: 30 June 2022

DOI: 10.1002/cta.3374

WILEY

ORIGINAL PAPER

Experimental evaluation of type-2 fuzzy logic controller adapted to real environmental conditions for maximum power point tracking of solar energy systems

Ahmet Gani[1] | **Mustafa Sekkeli**[2]

[1]Faculty of Engineering, Architecture and Design, Department of Electrical and Electronics Engineering, Kayseri University, Kayseri, Turkey

[2]Faculty of Engineering and Architecture, Department of Electrical and Electronics Engineering, Kahramanmaras Sutcu Imam University, Kahramanmaras, Turkey

Correspondence
Ahmet Gani, Faculty of Engineering, Architecture and Design, Department of Electrical and Electronics Engineering, Kayseri University, Kayseri 38280, Turkey.
Email: ahmetgani@kayseri.edu.tr

Funding information
Kahramanmaras Sutcu Imam University, Scientific Research Projects Unit, Grant/Award Number: 2018/5-11 D

Abstract

The conventional angle of incremental conductance (AIC) method fails to track the maximum power point (MPP) when a rapid change in solar irradiation and/or panel temperature appears because it cannot distinguish between rapid changes in photovoltaic (PV) current and voltage under real environmental conditions. The present study describes setbacks of the conventional AIC method and proposes an effective approach based on the combination of AIC and type-2 fuzzy. The proposed approach offers a significant advantage in terms of maximum power transfer to the load under long-term weather patterns under which broken clouds appear frequently during a 40-m testing period. The proposed approach is installed on 250 W module of a 10 kWp real PV plant in Kahramanmaras Sutcu Imam University. Later, its performance is validated by dSPACE1104 controller card operating in real time with MATLAB/Simulink tools using daily measured data. The experimental results obtained from the laboratory setup based on dSPACE1104 controller card demonstrate the facility and feasibility of the proposed approach for real PV plant with boost power converter and load.

KEYWORDS

long-term weather pattern, MPPT, solar energy, type-2 fuzzy

1 | INTRODUCTION

In today's world, the need for renewable energy sources has significantly increased due to the high level of demand for different energy sources. Solar energy comes to the forefront among various renewable energy sources because of its reliability and cleanliness.[1] Solar power plants (SPPs) have high installation cost due to components of the plant including PV module, DC–DC power converter, and energy storage devices in off-grid and on-grid operation.[2] The efficiency of SPPs is still limited to around 15% to 25%.[3] Therefore, it is essential to operate the SPPs at maximum power point (MPP). However, operating SPPs at the MPP is a very challenging task because they have nonlinear current–voltage (I–V) and power–voltage (P–V) characteristics depending on environmental conditions.[4–7] To cope with this situation and assure stability, the proposed effective approach can be defined as two-stage control scheme.[8,9] First, the MPP of PV module is determined. In the second stage, the maximum output power to the reference power is regulated.[10–12] Angle of incremental conductance (AIC) is one of the well-known stages which determine the MPP. However, the number of studies[13–17] using this method is limited, and a few studies have been carried out according to the latest

 © 2022 John Wiley & Sons Ltd.

literature survey. On the other hand, many intelligent maximum power point tracking (MPPT) methods such as sliding mode, fuzzy logic, and neural network have been proposed by various researchers to regulate stages.[18–28] Conventional fuzzy logic and fuzzy sets are called type-1 fuzzy logic systems (T1FLSs). T1FSs have been improved by Zadeh with a new concept called type-2 fuzzy logic systems (T2FLSs).[29] From a theoretical perspective, an effective MPPT is the ratio of the practical power output to the true maximum power value. However, it is not always easy to find an optimal MPPT method, since the accurate MPP varies at specific moments during the system operation. Table 1 summarizes the cited and previously proposed MPPT evaluation to provide an overview of various approaches that have been so far used to evaluate MPPT methods.[40]

The output power of PV module directly relies on solar irradiation and panel temperature which may suddenly change under actual weather conditions and lead to noise and uncertainties in the operation of a PV module. In the present study, the maximum power is determined using AIC method, and interval type-2 fuzzy logic (IT2FL) controller is proposed to close PV maximum output power to reference power through dealing with noise and uncertainties in the regulating stage. An experimental model was designed to measure the effectiveness of the proposed approach. Later, an experimental setup was developed using dSPACE 1104 control card to apply the proposed approach in real time.

Given other experimental studies in the literature, the main contributions of the present study can be summarized as follows:

* Long-term weather pattern using natural sunlight is proposed to converge to actual working conditions and offers a more accurate evaluation for MPPT dynamic performance evaluation.
* The performance of proposed approach is validated using a laboratory setup based on dSPACE1104 controller card.
* The proposed controller overcomes the disturbance caused by environmental changes and deals with measurement noise under real environmental conditions.
* The transient and steady-state responses of the proposed approach at any time are effective in the presence of long-term weather pattern evaluation.
* The actual behavior of the proposed controller is analyzed using real PV module and natural sunlight to eliminate any unrealistic effects caused by artificial sunlight and PV array simulator.

In the present study, solar energy conversion system (SECS) is described in Section 2. The design of the proposed control structure is presented in Section 3. Experimental assessments are analyzed in Section 4. The findings are concluded in Section 5.

2 | SECS

The SECS contains a PV generator and an equivalent load. The controlled power block between PV generator and resistive load is shown in Figure 1.

TABLE 1 A summary of MPPT evaluation methods

Evaluation method	Comment
Simulation[30]	- Cost-effectiveness and test condition flexibility - Does not offer experimental evaluation
PV array simulator[31–33]	- Provides power source to alternate true PV array - Relatively moderate cost and flexibility for different test conditions - Does not offer experimental evaluation under natural sunlight
Artificial light[34–36]	- Offers controllable radiation - High cost for a high power test with similar solar spectrum - Problematic and uncontrollable PC cell temperature
Natural sunlight[37–39]	- Operates under natural sunlight - Offers an accurate evaluation for steady weather conditions such as solar irradiance and ambient temperature - Does not evaluate fast MPPT dynamics caused by moving clouds - Offers a long-term test to adapt to different weather conditions

1097007x, 2022, 11, Downloaded from https://onlinelibrary.wiley.com/doi/10.1002/cta.3374 by Kayseri University, Wiley Online Library on [02/01/2024]. See the Terms and Conditions (https://onlinelibrary.wiley.com/terms-and-conditions) on Wiley Online Library for rules of use; OA articles are governed by the applicable Creative Commons License

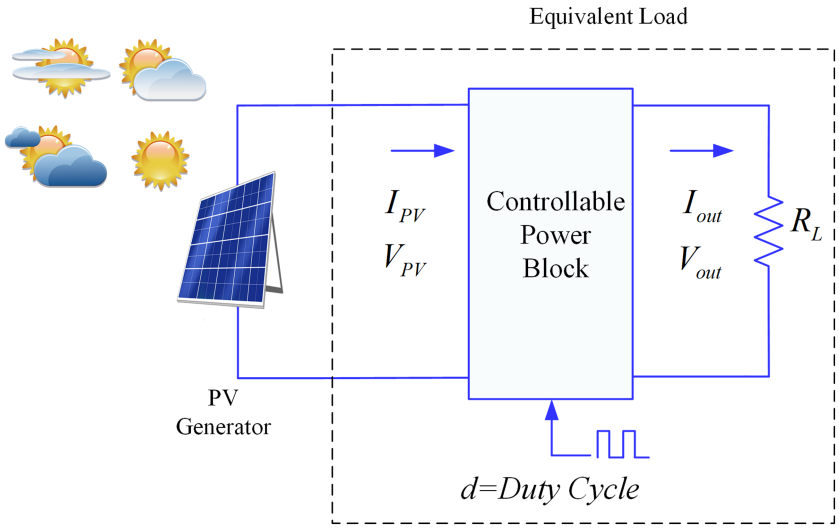


FIGURE 1 The controlled power block between PV generator and resistive load

MPPT methods mainly aim to find an impedance match between the PV generator and resistive load through a controllable power block. It can be seen in Figure 1 that the controllable power block and resistive load can be considered as an equivalent load. In general, the controllable power block includes DC–DC power converters. In this case, when I_{PV} and V_{PV} are input current and voltage, respectively, I_{out} and V_{out} denote output current and voltage. Finally, d represents the duty cycle of the DC–DC power converter.[41] If DC–DC converter is ideal, DC–DC power converter is expressed in Equation (1):

$$R_{PV} = \frac{R_L}{M(d)^2}. \tag{1}$$

Here, R_{PV} and R_L are the impedance of the PV generator and resistive load, respectively. $M(d)$ is the voltage conversion ratio. On the other hand, when the boost power converter is used as the controllable power block, its $M(d)$ can be calculated as follows:

$$M(d) = \frac{V_{out}}{V_{PV}} = \frac{1}{1-d}. \tag{2}$$

When (2) is substituted by (1), the relationship between R_{PV} and R_L can be defined as

$$R_{PV} = R_L(1-d)^2. \tag{3}$$

In this equation, the term $R_L(1-d)^2$ refers to the equivalent load, while d is the duty cycle. It is possible to change the equivalent load by adjusting the value of d, which allows locating the movement of maximum operating points.[42]

3 | DESIGN OF PROPOSED CONTROL STRUCTURE

Interval type-2 fuzzy logic system (IT2FLS) is used to reduce the computational cost of T2FLSs. IT2FLSs can be categorized into two types as Mamdani and Takagi–Sugeno–Kang (TSK) depending on the rules. The consequent parts of an IT2-TSK-FLS and Mamdani IT2FLS consist of linear functions and membership function, respectively.[43,44] The IT2-TSK-FLS is divided into three different models based on the consequent of the type of rule: A2-C0, A2-C1, and A2-C2.[45] The TSK rule is called an A2-C0 case if the antecedents are IT2FLSs and its consequents are crisp numbers.

1097007x, 2022, 11, Downloaded from https://onlinelibrary.wiley.com/doi/10.1002/cta.3374 by Kayseri University, Wiley Online Library on [02/01/2024]. See the Terms and Conditions (https://onlinelibrary.wiley.com/terms-and-conditions) on Wiley Online Library for rules of use; OA articles are governed by the applicable Creative Commons License

Due to its simplicity and lower computational cost compared to other types, the present study benefits from the IT2 A2-C0 TSK fuzzy model. The systematic framework of IT2 A2-C0 TSK fuzzy model is shown in Figure 2.

Figure 2 shows the systematic framework of the IT2 A2-C0 TSK fuzzy model. In this model, the input variables are the error signal $e(k)$ and the change of error signal $de(k)$, while the output variable is the change of duty cycle $\Delta d(k)$ is. The error signal $e(k)$, the change of error signal $de(k)$, and duty cycle $d(k)$ are calculated as follows:

$$e(\mathrm{k}) = \tan^{-1}\left(\frac{I_{pv}}{V_{pv}}\right) + \tan^{-1}\left(\frac{dI_{pv}}{dV_{pv}}\right), \tag{4}$$

$$de(k) = e(k) - e(k-1). \tag{5}$$

In this equation, $e(k)$ and $e(k-1)$ denote the current and previous samples of the error variable, respectively. Thus, AIC method generates the $e(k)$ and $de(k)$ values using the measured output current and voltage of the PV module.

$$d(k) = d(k-1) + \Delta d(k). \tag{6}$$

$d(k-1)$ is the previous output, whereas $\Delta d(k)$ is the change in the output variable. The structure of the IT2 A2-CO TSK fuzzy model is as follows: The inputs called crisp input are fuzzified using the fuzzification process in type-2 fuzzy sets. Then, the inference engine generates a type-2 fuzzy output using rule base. The output processing creates the crisp output Δd(k). Gaussian type-2 fuzzy sets with uncertain standard deviation (SD) are the most common membership functions in IT2 A2-C0 TSK fuzzy models,[46,47] which can be defined as follows:

$$\mu_{\tilde{G}}(x) = \exp\left\{-\frac{1}{2}\left(\frac{x-c}{\sigma_{ij}}\right)^2\right\}, \sigma_{ij} \in \left[\overline{\sigma}_{ij}, \underline{\sigma}_{ij}\right]. \tag{7}$$

Here, x and c denote the input variable and center value of MF, respectively. $\overline{\sigma}_{ij}$ and $\underline{\sigma}_{ij}$ represent the SD for the upper MF (UMF) and lower MF (LMF). Gaussian type-2 fuzzy set is shown in Figure 3.

Footprint of uncertainty (FOU) shown in Figure 3 is the limited domain representing the primary uncertainty of type-2 fuzzy set between UMF and LMF. The rule base structure of IT2-TSK-FLS for the A2-C0 case is expressed as follows:

$$Rule^i : IF\ e(k)\ is \tilde{A}_1^{\ i}\ and\ de(k)\ is \tilde{A}_2^{\ i}\ then\ \Delta d_i(k) = a_1^{\ i} e(k) + a_2^{\ i} de(k). \tag{8}$$

Here, $i = 1, ..., M$ represents the number of rules. The M is selected as 25. $\tilde{A}_j^{\ i}$ is the input variable j in rule and i. $a_1^{\ i}$ and $a_2^{\ i}$ are the consequent parameters. The upper and lower firing strengths of the rules for the ith rule, $\overline{f^i}$ and $\underline{f^i}$ are calculated as follows:

$$\overline{f^i} = \overline{\mu}_{\tilde{A}_1^{\ i}}(e(k)) * \overline{\mu}_{\tilde{A}_2^{\ i}}(de(k)), \tag{9}$$

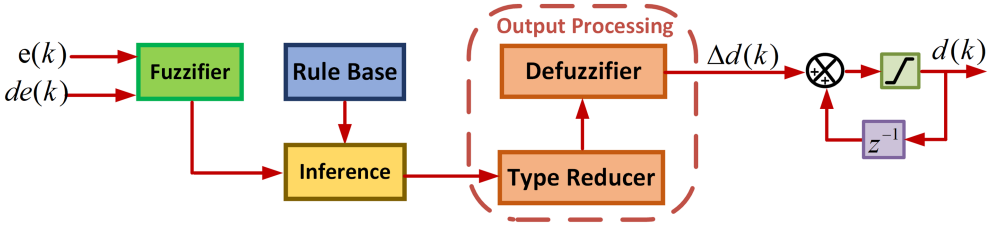


FIGURE 2 The systematic framework of IT2 A2-C0 TSK fuzzy model

1097007x, 2022, 11, Downloaded from https://onlinelibrary.wiley.com/doi/10.1002/cta.3374 by Kayseri University, Wiley Online Library on [02/01/2024]. See the Terms and Conditions (https://onlinelibrary.wiley.com/terms-and-conditions) on Wiley Online Library for rules of use; OA articles are governed by the applicable Creative Commons License

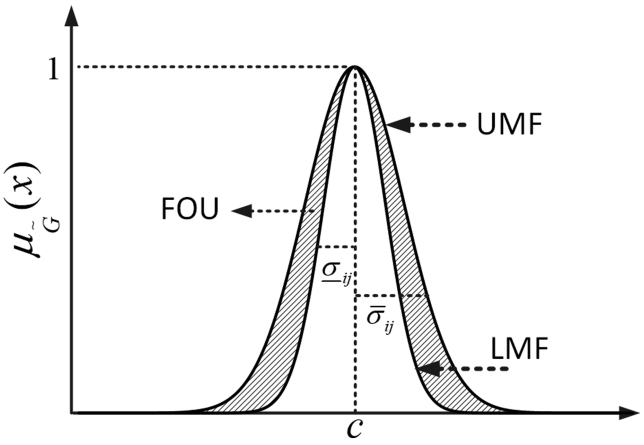


FIGURE 3 Gaussian type-2 fuzzy set

$$\underline{f}^i = \underline{\mu}_{\underset{\sim}{A}_1{}^i}(e(k)) * \underline{\mu}_{\underset{\sim}{A}_2{}^i}(de(k)), \tag{10}$$

where * is product *t*-norm operator. $\overline{\mu}_{\underset{\sim}{A}_j{}^i}$ and $\underline{\mu}_{\underset{\sim}{A}_j{}^i}$ $j = 1,2$ indicate the UMF and LMF of the rule i, respectively. Normalization process is performed by proportioning the firing strength of each node rule to the sum of the firing strengths of all rules.[48,49] This process is given in the following equations:

$$\overline{F}^i = \frac{\overline{f}^i}{\sum \overline{f}^i}, \tag{11}$$

$$\underline{F}^i = \frac{\underline{f}_i}{\sum \underline{f}_i}, \tag{12}$$

As Biglarbegian–Melek–Mendel (BMM) method[50] requires less computation for type reduction and defuzzification, it is used in output processing, as given below:

$$\Delta d_L(k) = \frac{\sum_{i=1}^{M} \overline{F^i} \Delta d_i(k)}{\sum_{i=1}^{M} \overline{F^i}}, \tag{13}$$

$$\Delta d_R(k) = \frac{\sum_{i=1}^{M} \underline{F_i} \Delta d_i(k)}{\sum_{i=1}^{M} \underline{F_i}}, \tag{14}$$

$$\Delta d(k) = q\Delta d_L(k) + (1-q)\Delta d_R(k). \tag{15}$$

Input membership functions of the IT2-TSK-FLC are shown in Figure 4.

Here, q is a design parameter which weighs the sharing of lower and upper firing levels in the defuzzification output. Thanks to the BMM method, this parameter is restricted to [0, 1]. The value of q is selected as 0.6 in the present study. The implementation steps of the proposed controller are described below and shown in Figure 5.

Step 1: The IT2-TSK-FLC parameters such as the input membership functions and rule base structure are defined via error and change of error signal.

1097007x, 2022, 11, Downloaded from https://onlinelibrary.wiley.com/doi/10.1002/cta.3374 by Kayseri University, Wiley Online Library on [02/01/2024]. See the Terms and Conditions (https://onlinelibrary.wiley.com/terms-and-conditions) on Wiley Online Library for rules of use; OA articles are governed by the applicable Creative Commons License

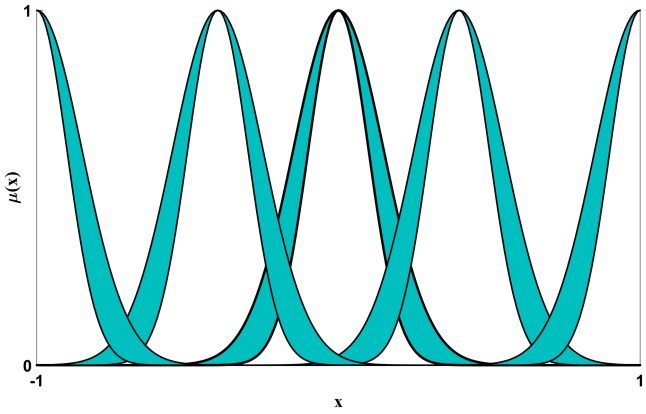


FIGURE 4 Input membership functions of the IT2-TSK-FLC

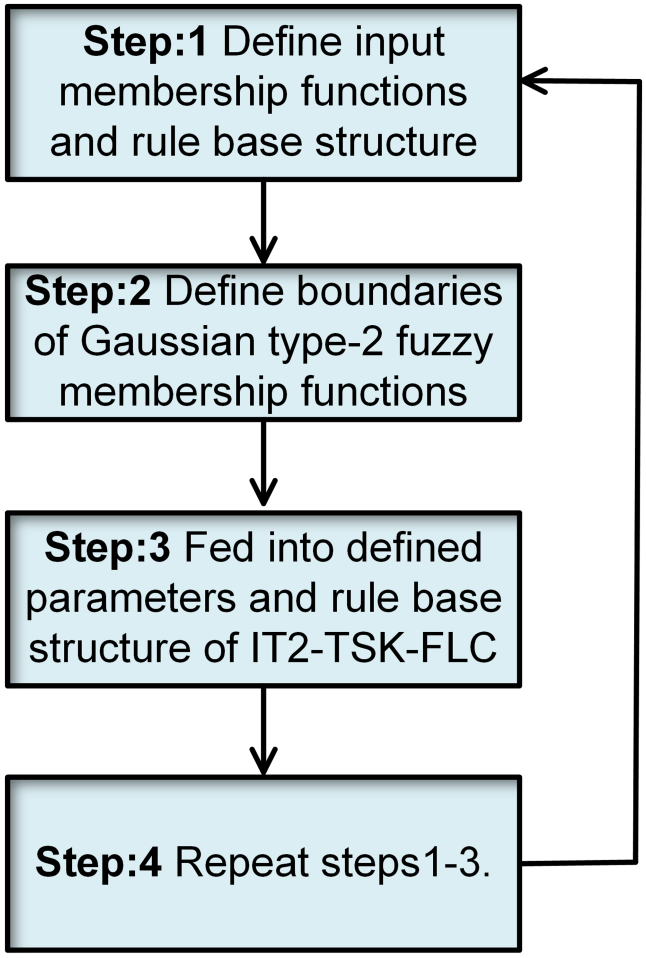


FIGURE 5 The steps of proposed controller implementation

Step 2: The boundaries of input Gaussian type-2 membership functions are determined based on the system parameters and the required system response.
Step 3: The defined parameters and rule base structure are fed into the proposed IT2-TSK-FLC controller that outputs the duty cycle for the boost power converter.
Step 4: Repeat Step 1–3.

1097007x, 2022, 11, Downloaded from https://onlinelibrary.wiley.com/doi/10.1002/cta.3374 by Kayseri University, Wiley Online Library on [02/01/2024]. See the Terms and Conditions (https://onlinelibrary.wiley.com/terms-and-conditions) on Wiley Online Library for rules of use; OA articles are governed by the applicable Creative Commons License

4 | EXPERIMENTAL EVALUATIONS

MPPT control mainly aims to track maximum power under certain environmental conditions such as solar radiation, ambient temperature, and cloud shading.[51–53] It requires an experimental prototype for the analysis of MPPT performance in terms of solar energy harvest for a long period of time. In addition, long-term evaluation under natural sunlight is also essential to test the performance of an effective MPPT algorithm without exposure to side effects of power electronic-based PV simulators and artificial light sources. In this section, an experimental prototype is proposed, and related issues are discussed to evaluate its MPPT performance accurately. For a healthier evaluation of the proposed controller, a dSPACE1104 controlled PV power system was designed and constructed. To this end, the electrical parameters of PV module and selected values for the DC–DC power converter are given in Tables 2 and 3.

The circuit output is controlled by the duty cycle of the power semiconductor IGBT device, which is controlled through the pulse-width modulation (PWM). In order to maximize the output power of the SECS, the converter duty cycle is the most significant element in selecting boost converter components and controlling DC–DC power converter. The proposed boost DC–DC power converter in the present study provides voltage boost and continuous current mode for the PV module side. Experimental prototype based on dSPACE1104, which was developed in the laboratory, could operate with MATLAB/Simulink environment in real time. The actual PV parameters were collected from a PV plant with an installed power 10 kWp at Kahramanmaras Sutcu Imam University during the day to measure the performance of the proposed controller under real environmental conditions. A view of the PV plant in question is shown Figure 6 to evaluate the performance of the proposed approach.

The experimental setup for the proposed approach is shown in Figure 7.

Figure 7 demonstrates the experimental setup for the proposed approach. "1" is the interface of ControlDesk software used to display the measured graphical and numerical parameters in real time. "2," "3," "4," "5," "6," and "7" are digital oscilloscope, dSPACE1104 controller card, voltage probes, DC–DC boost power converter, variable resistor, and current probes, respectively. The PV module is placed on the top of the SPP in Figure 7. In addition, a schematic depiction of the experimental study can be seen in Figure 8.

As shown in Figure 8, current and voltage sensing devices must be highly accurate and sensitive for hardware implementation of MPPT. Therefore, current and voltage values of PV module were measured using PICO TA018 current probe and PINTEK DP-25 voltage probes. The measured PV module current and voltage values were applied to analog–digital converters (ADCs) of the DS1104 controller card. Additionally, ADC block current and voltage values were scaled. Later, the calculated current and voltage values were applied to the proposed control structure in MATLAB/Simulink. DSP PWM signals obtained from the control algorithm were applied to the gate driver circuit and later sent to IGBT for switching process. In this respect, to supply the suitable gate signal, DSP PWM signals coming

TABLE 2 Electrical characteristic parameters of PV module

Optimum operating voltage	V_{MP}	31.28 V
Optimum operating current	I_{MP}	8.01 A
Open-circuit voltage	V_{oc}	37.66 V
Short-circuit current	I_{sc}	8.66 A
Rated power of PV module	P_{max}	250 W
Panel efficiency	η	15.4%

TABLE 3 The selected values of boost DC–DC power converter

Toroidal ferrite core	L	10 mH
Electrolytic capacitor	C	220 μF
IGBT	V_{IGBT}, I_{IGBT}	600 V–23 A
Load resistance	R_L	40 Ω
Switching frequency	f	20 kHz
PV capacitor	C_{PV}	330 μF

1097007x, 2022, 11, Downloaded from https://onlinelibrary.wiley.com/doi/10.1002/cta.3374 by Kayseri University, Wiley Online Library on [02/01/2024]. See the Terms and Conditions (https://onlinelibrary.wiley.com/terms-and-conditions) on Wiley Online Library for rules of use; OA articles are governed by the applicable Creative Commons License



FIGURE 6 A view of PV plant

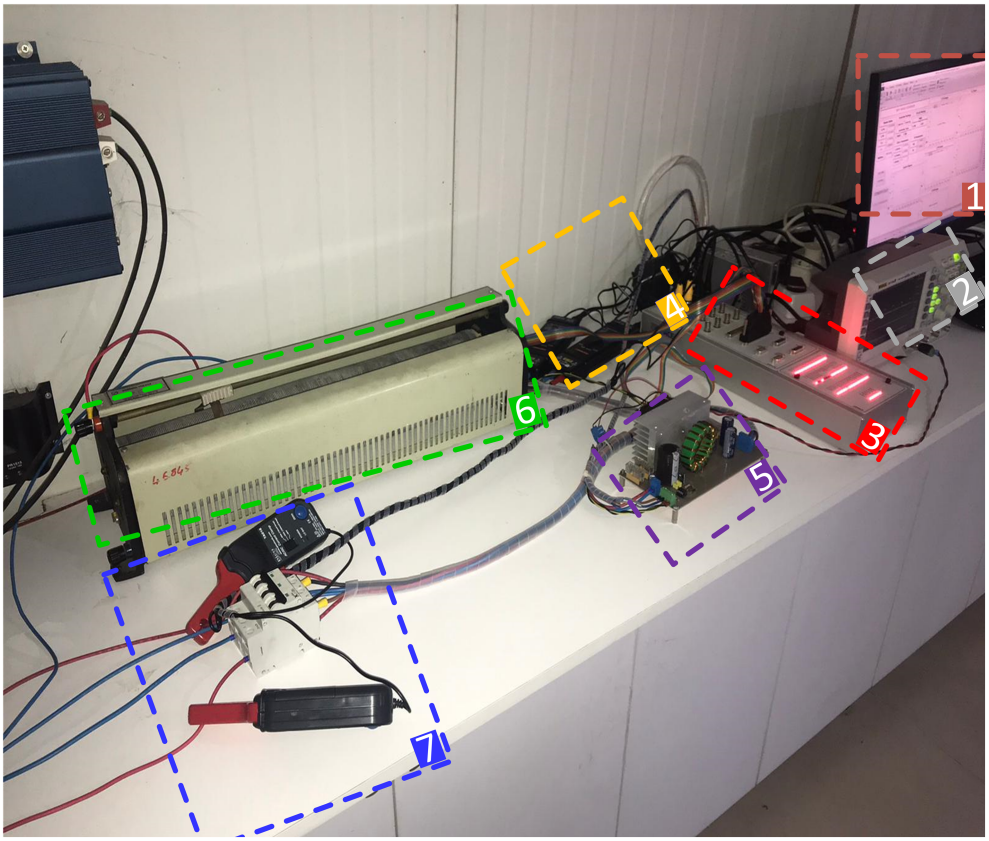


FIGURE 7 The experimental setup for the proposed approach

from the controller card needed to be increased for IGBT, that is, the switching element. In addition, DSP control card output was protected by isolating the gate of IGBT and DSP PWM outputs. Figure 9 indicates the gate driver circuit designed for the present study.

It can be seen in Figure 9 that a HCPL 3120 optocoupler with an output power of 2.5 ampere was used as a gate driver, since it yielded a more stable output at a higher switching frequency. The proposed control structure in the experimental study was designed using MATLAB/Simulink and converted to real-time codes via Simulink Real-Time Workshop and DSPACE Real-Time Interface (RTI) software. A dSPACE DS1104 controller card compatible with MATLAB/Simulink was also used. Its main satellite processors are PowerPC PPC603e/250 MHz and Texas Instruments TMS320F240/20 MHz. Thanks to ControlDesk software developed by DSPACE, real-time waveforms obtained from the system were monitored. The designed RTI model in the experimental study is shown in Figure 10.

1097007x, 2022, 11, Downloaded from https://onlinelibrary.wiley.com/doi/10.1002/cta.3374 by Kayseri University, Wiley Online Library on [02/01/2024]. See the Terms and Conditions (https://onlinelibrary.wiley.com/terms-and-conditions) on Wiley Online Library for rules of use; OA articles are governed by the applicable Creative Commons License

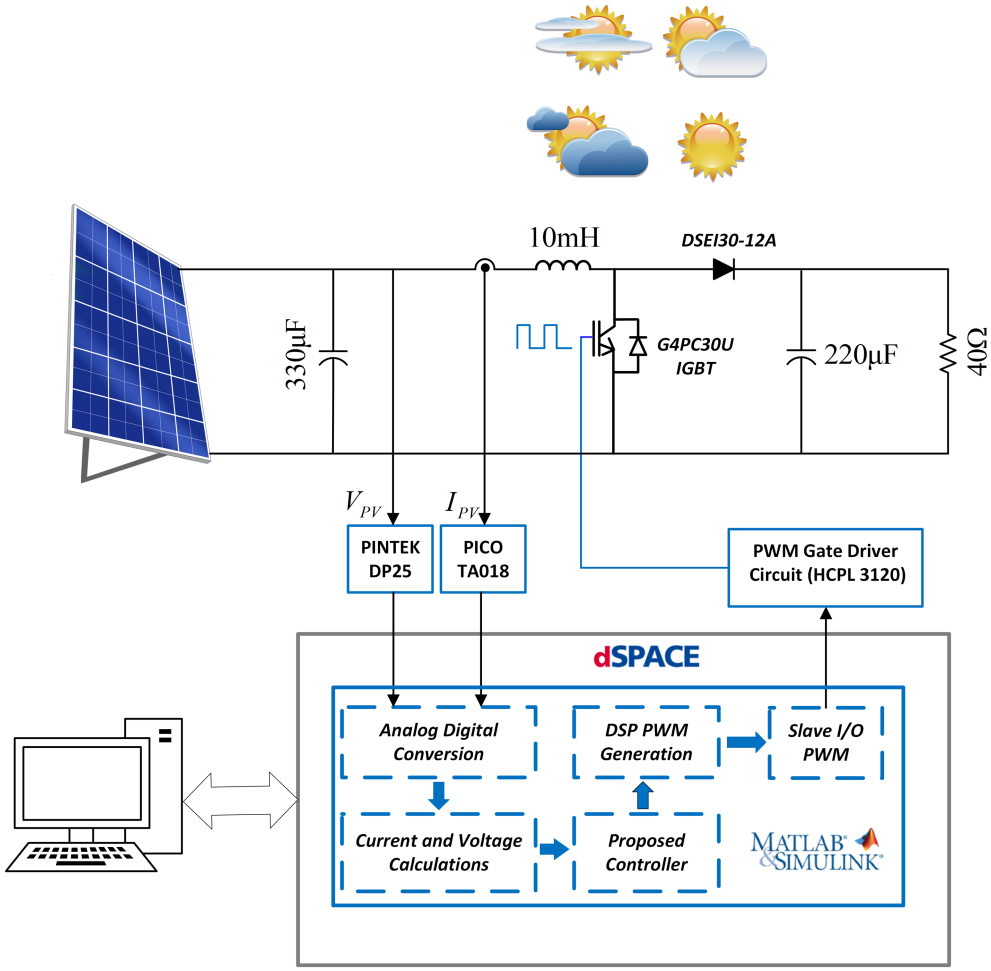


FIGURE 8 A schematic depiction of the experimental approach

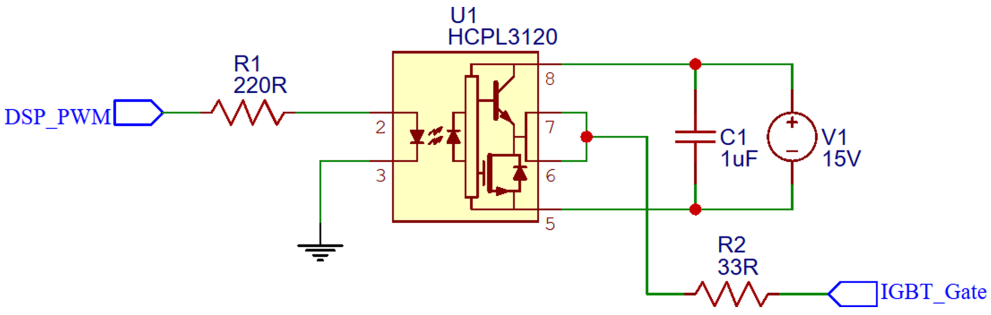


FIGURE 9 Gate driver circuit

The saturation block on the RTI model functioned as software protection for duty cycle of PWM signal, as shown in Figure 10. The lower and upper limits of this block were adjusted to 0.2 and 0.8, respectively. Afterwards, they were applied to IGBT for the switching process. Sampling time was 100 μs for RTI model. However, for the real-time analysis, a PV capacitor was placed between PV panel and boost DC–DC power converter to reduce any current and voltage fluctuation. The experimental study was conducted on 22/11/2019. Solar irradiance and panel temperature values obtained from EVO PVI-AEC-IRR T data logger are shown in Figure 11.

During the experimental study, a maximum output power was obtained from PV module under sudden changes in environmental conditions between 11:40 and 12:20 to analyze the performance of the proposed structure. After 37.18 s elapsed, the PWM signal was applied to gate driver circuit using the "PWM START/STOP" block on the RTI model.

1097007x, 2022, 11, Downloaded from https://onlinelibrary.wiley.com/doi/10.1002/cta.3374 by Kayseri University, Wiley Online Library on [02/01/2024]. See the Terms and Conditions (https://onlinelibrary.wiley.com/terms-and-conditions) on Wiley Online Library for rules of use; OA articles are governed by the applicable Creative Commons License

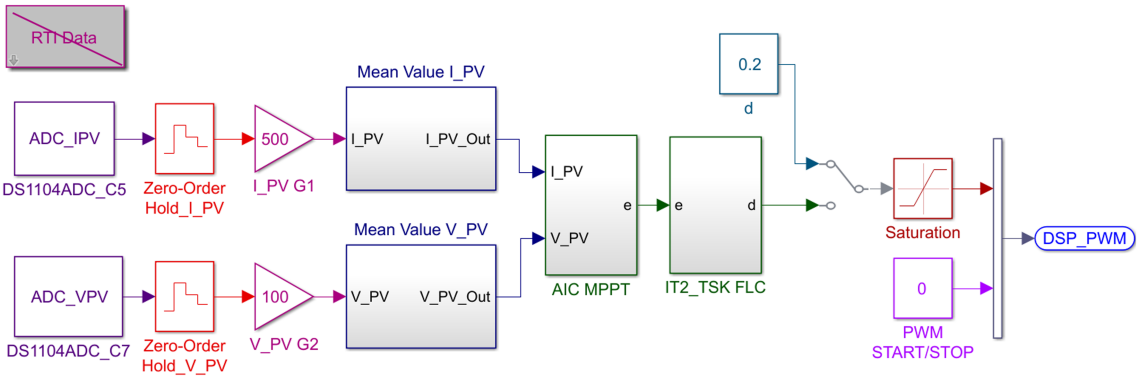


FIGURE 10 The designed RTI model for the experimental evaluation

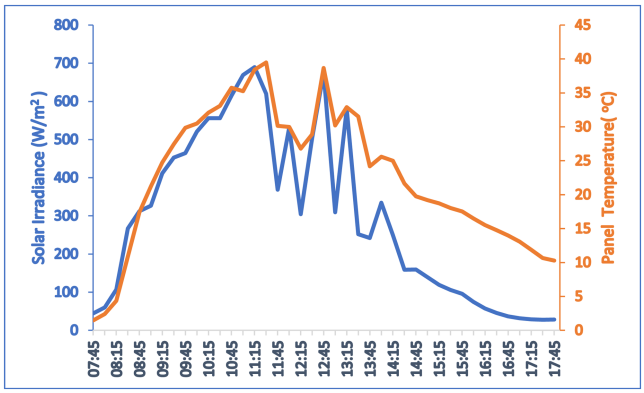


FIGURE 11 The actual solar irradiance and panel temperature values

Experimental results obtained from the laboratory setup based on dSPACE1104 controller card can be seen in Figure 12.

The current and voltage values of the PV module during the experimental study can be seen in Figure 12A,B, respectively. As shown in Figure 12A, the PV current value decreased from 6.59 to 2.48 A simultaneously with sudden clouding which started from the 1000th second. The peak current value obtained from PV module was 7.017 A. Figure 12B clearly demonstrates that PV voltage value increased from 27.49 to 30.11 V simultaneously with the decreasing panel temperature. The peak voltage value obtained from PV module was 35.02 V. Despite sudden clouding, the proposed controller managed to maintain the PV voltage value almost around the MPP value. The PV panel power and control signal of the proposed controller are shown in Figure 12C,D, respectively. As shown in Figure 12C, the power value of PV module decreased from 179.2 to 74.47 W simultaneously with sudden clouding which started at the 1000th second. The peak power value was 183.5 W. Thus, it is evident that the proposed controller determined the proper duty cycle applied to boost DC–DC power converter successfully to generate maximum power from PV module. It is widely acknowledged that solar irradiance and cell temperature are two key parameters which heavily affect the PV power output in terms of output voltage and current. The control signal of the proposed controller can be seen in Figure 12D. Due to sudden changes in irradiance, the MPP reaches another new point that, in turn, changes the value of e (an input error for the controller). Steady-state performance is also difficult to evaluate because the true MPP is not likely to be determined during a real-time test under natural sunlight. The controller brings the e to a minimum value by changing the d for any new operating point. It must be noted that the PV current and power vary remarkably during a testing period. The output voltage of DC–DC power converter is given in Figure 12E. As shown in Figure 12E, DC–DC power converter had a durable output voltage which shows robustness of converter. The waveforms for SECS such as PV power, voltage, current, and output voltage waveforms obtained from a digital oscilloscope at any steady-state operating point are shown in Figure 13. The PWM waveform of the designed boost DC–DC power converter obtained from a digital oscilloscope is shown in Figure 14.

1097007x, 2022, 11, Downloaded from https://onlinelibrary.wiley.com/doi/10.1002/cta.3374 by Kayseri University, Wiley Online Library on [02/01/2024]. See the Terms and Conditions (https://onlinelibrary.wiley.com/terms-and-conditions) on Wiley Online Library for rules of use; OA articles are governed by the applicable Creative Commons License

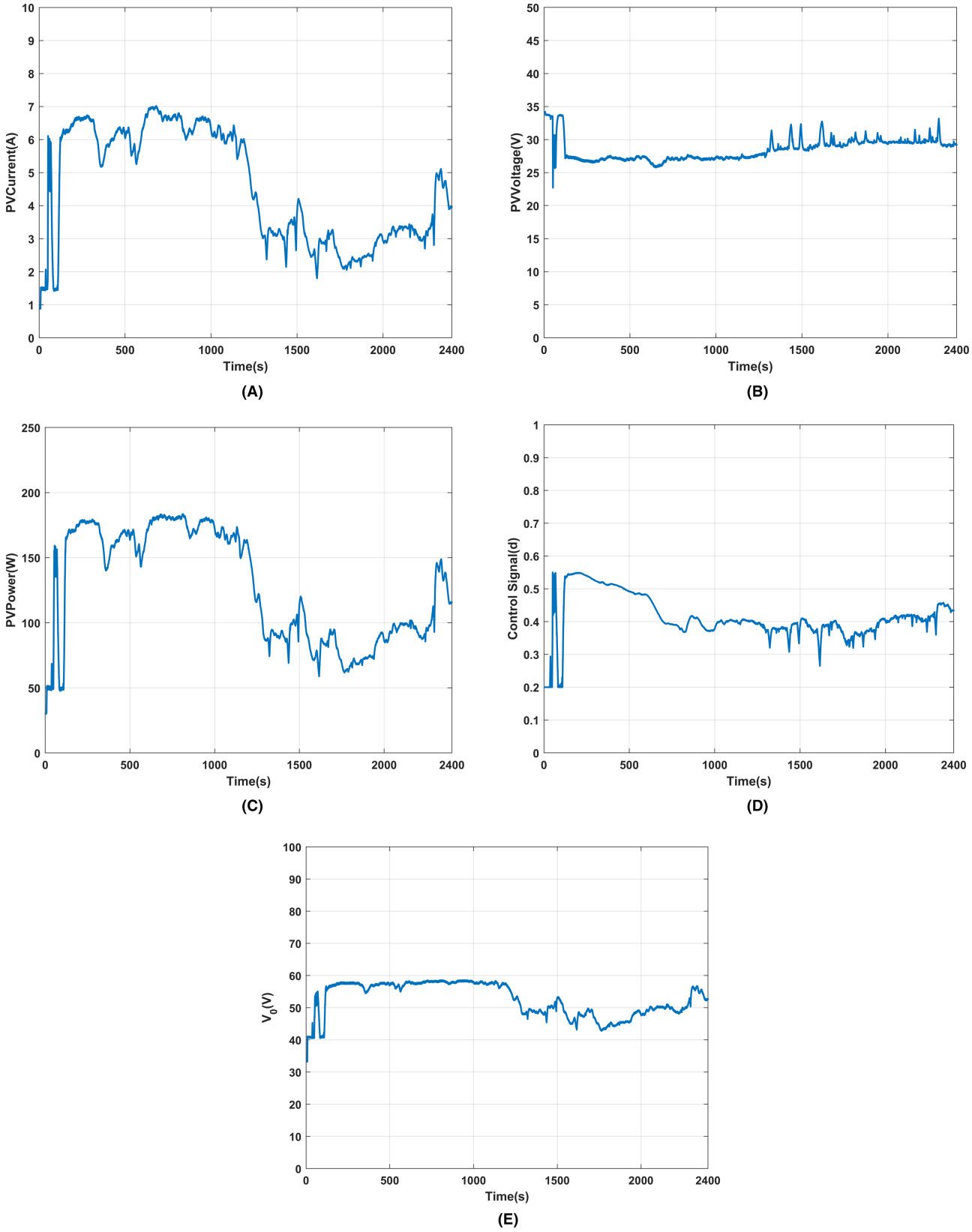


FIGURE 12 (A) Experimental current of PV module. (B) Experimental voltage of PV module. (C) Experimental power of PV module. (D) Control signal of proposed controller. (E) Output voltage of DC–DC converter

1097007x, 2022, 11, Downloaded from https://onlinelibrary.wiley.com/doi/10.1002/cta.3374 by Kayseri University, Wiley Online Library on [02/01/2024]. See the Terms and Conditions (https://onlinelibrary.wiley.com/terms-and-conditions) on Wiley Online Library for rules of use; OA articles are governed by the applicable Creative Commons License

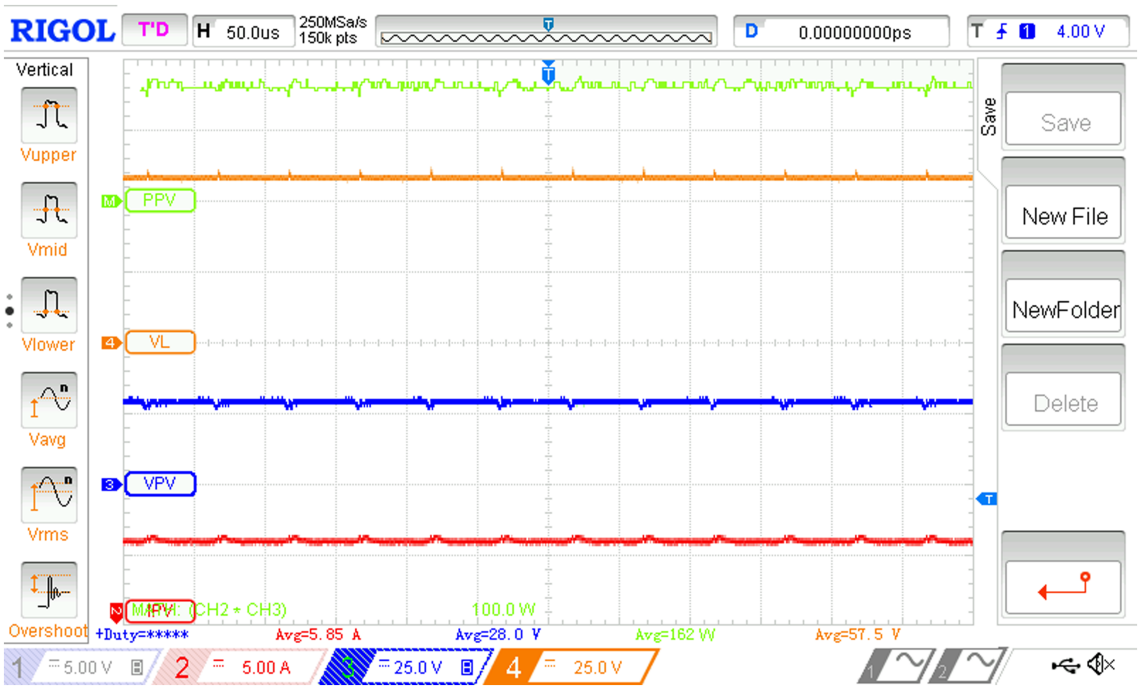


FIGURE 13 The waveforms for SECS obtained from digital oscilloscope at any steady-state operating point

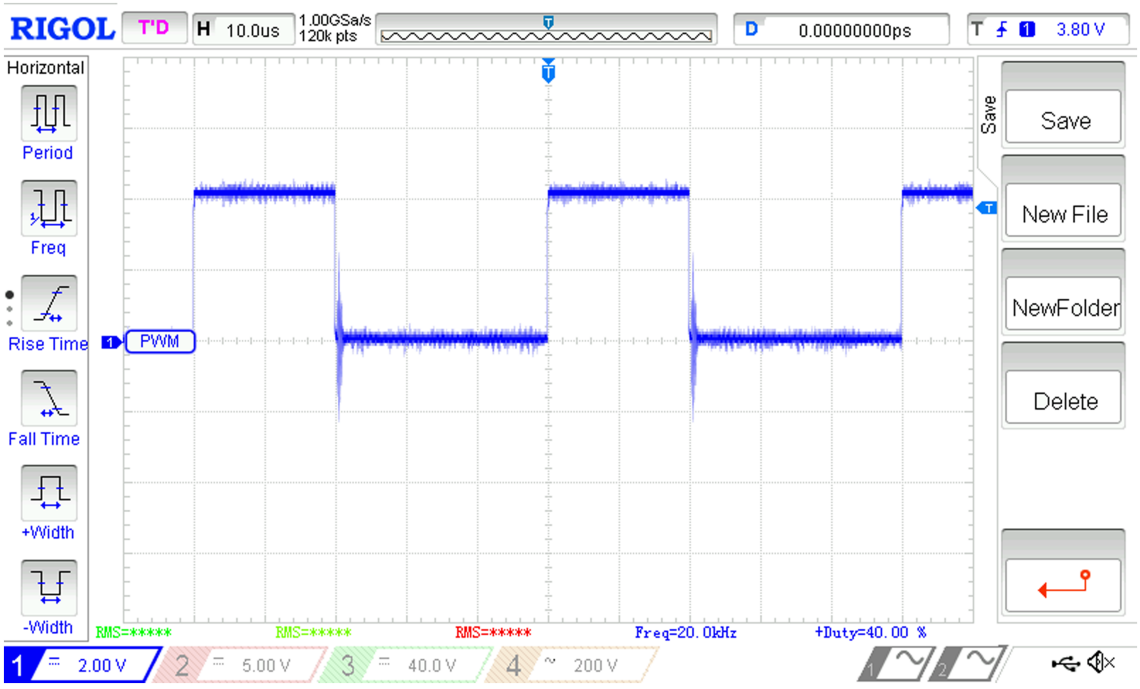


FIGURE 14 The PWM waveform of the designed boost DC–DC power converter obtained from a digital oscilloscope

It is evident from Figure 13 that at any steady-state operating point, the proposed controller reaches the maximum output values for the PV module. Additionally, the proposed controller can obtain mitigated fluctuations at any steady-state operating point.

1097007x, 2022, 11, Downloaded from https://onlinelibrary.wiley.com/doi/10.1002/cta.3374 by Kayseri University, Wiley Online Library on [02/01/2024]. See the Terms and Conditions (https://onlinelibrary.wiley.com/terms-and-conditions) on Wiley Online Library for rules of use; OA articles are governed by the applicable Creative Commons License

TABLE 4 The minimum and maximum values obtained from PV module via the proposed controller

Parameters	Min–max values
PV current	0.8756–7.017 A
PV voltage	22.71–35.02 V
PV power	29.93–183.5 W

The results obtained from Figure 14 confirm that proper design of the boost power stage and stable performance of the proposed controller. Table 4 presents the minimum (min) and maximum (max) values obtained from PV module with the proposed controller.

As can be understood from Table 4, the min–max values obtained from PV module under transient and steady-state operating conditions demonstrate that the proposed controller could extract optimal PV current, voltage, and power values from the PV module.

5 | CONCLUSION

The present study proposes an intelligent control structure based upon IT2-TSK-FLC to extract MPP of SECS and reduce power fluctuations at transient and steady-state operating points. IT2-TSK-FLC contains an effective and durable control structure which adapts to unstable environmental conditions rapidly. An experimental study was conducted during a long-term weather period of the day to analyze the stability and dynamic performance of the proposed control structure. The experimental results clearly demonstrated that the proposed controller succeeded in extracting an optimal power from the PV module under unstable weather conditions and thus performed effectively. In future studies, it is aimed to apply the proposed approach to grid-tied solar energy systems.

ACKNOWLEDGMENT

This work was financially supported by the Kahramanmaras Sutcu Imam University, Scientific Research Projects Unit, the project entitled "Optimal Control and Implementation of Maximum Power Point in Photovoltaic Systems" under Project No: 2018/5-11 D.

DATA AVAILABILITY STATEMENT

Research data are not shared.

REFERENCES

1. Keçecioğlu OF, Acikgoz H, Gani A. Fuzzy-PI based MPPT control for photovoltaic systems. In: *2018 Innovations in Intelligent Systems and Applications Conference (ASYU)*. IEEE; 2018:1-4.
2. Basha CH, Murali M. A new design of transformerless, non-isolated, high step-up DC-DC converter with hybrid fuzzy logic MPPT controller. *Int J Circuit Theory Appl*. 2022;50(1):272-297. doi:10.1002/cta.3153
3. Celikel R, Boztas G, Aydogmus O. A system identification-based MPPT algorithm for solar photovoltaic pumping system under partial shading conditions. *Energy Sources A: Recovery Util Environ Eff*. 2022;44(2):5199-5214. doi:10.1080/15567036.2022.2083274
4. Gani A. Improving dynamic efficiency of photovoltaic generation systems using adaptive type 2 fuzzy-neural network via EN 50530 test procedure. *Int J Circuit Theory Appl*. 2021;49(11):3922-3940. doi:10.1002/cta.3126
5. Kececioglu OF, Gani A, Sekkeli M. Improved hybrid intelligent controller design for MPPT of stand-alone PV system. *Turkish J Eng*. 2021;5(1):20-28. doi:10.31127/tuje.652229
6. Gani A, Acikgoz H, Sekkeli M. Maximum power point tracking with neuro-fuzzy controller under variable load and solar irradiance in photovoltaic systems. *Eur J Sci Tech*. 2020;(19):734-745. doi:10.31590/ejosat.748384
7. Chen M, Ma S, Wu J, Huang L. Analysis of MPPT failure and development of an augmented nonlinear controller for MPPT of photovoltaic systems under partial shading conditions. *Appl Sci*. 2017;7(1):95. doi:10.3390/app7010095
8. Ahmed M, Harbi I, Kennel R, Rodriguez J, Abdelrahem M. Model-based maximum power point tracking algorithm with constant power generation capability and fast DC-link dynamics for two-stage PV systems. *IEEE Access*. 2022;10:48551-48568. doi:10.1109/ACCESS.2022.3172292
9. Kandemir E, Cetin NS, Borekci S. Single-stage photovoltaic system design based on energy recovery and fuzzy logic control for partial shading condition. *Int J Circuit Theory Appl*. 2022;50(5):1770-1792. doi:10.1002/cta.3223

1097007x, 2022, 11, Downloaded from https://onlinelibrary.wiley.com/doi/10.1002/cta.3374 by Kayseri University, Wiley Online Library on [02/01/2024]. See the Terms and Conditions (https://onlinelibrary.wiley.com/terms-and-conditions) on Wiley Online Library for rules of use; OA articles are governed by the applicable Creative Commons License

10. Mojallizadeh MR, Badamchizadeh MA. Application of sliding-mode control for maximum power point tracking of PV systems. In: *Solar Photovoltaic Power Plants*. Springer; 2019:25-43. doi:10.1007/978-981-13-6151-7_2
11. Chiu CS, Ouyang YL, Ku CY. Terminal sliding mode control for maximum power point tracking of photovoltaic power generation systems. *Solar Energy*. 2012;86(10):2986-2995. doi:10.1016/j.solener.2012.07.008
12. Mojallizadeh MR, Badamchizadeh M, Khanmohammadi S, Sabahi M. Designing a new robust sliding mode controller for maximum power point tracking of photovoltaic cells. *Solar Energy*. 2016;132:538-546. doi:10.1016/j.solener.2016.03.038
13. Shiau JK, Wei YC, Chen BC. A study on the fuzzy-logic-based solar power MPPT algorithms using different fuzzy input variables. *Algorithms*. 2015;8(2):100-127. doi:10.3390/a8020100
14. Kececioglu OF, Gani A, Sekkeli M. Design and hardware implementation based on hybrid structure for MPPT of PV system using an interval type-2 TSK fuzzy logic controller. *Energies*. 2020;13(7):1842. doi:10.3390/en13071842
15. Kandemir E, Borekci S, Cetin NS. Conventional and soft-computing based MPPT methods comparisons in direct and indirect modes for single stage PV systems. *Elektronika Ir Elektrotechnika*. 2018;24(4):45-52. doi:10.5755/j01.eie.24.4.21477
16. Shiau JK, Wei YC, Lee MY. Fuzzy controller for a voltage-regulated solar-powered MPPT system for hybrid power system applications. *Energies*. 2015;8(5):3292-3312. doi:10.3390/en8053292
17. Kandemir E, Cetin NS, Borekci S. A comparison of perturb & observe and fuzzy-logic based MPPT methods for uniform environment conditions. *Period Eng Natural Sci*. 2017;5(1). doi:10.21533/pen.v5i1.67
18. Chu CC, Chen CL. Robust maximum power point tracking method for photovoltaic cells: a sliding mode control approach. *Solar Energy*. 2009;83(8):1370-1378. doi:10.1016/j.solener.2009.03.005
19. Zhang F, Maddy J, Premier G, Guwy A. Novel current sensing photovoltaic maximum power point tracking based on sliding mode control strategy. *Solar Energy*. 2015;118:80-86. doi:10.1016/j.solener.2015.04.039
20. Yau HT, Chen CL. Fuzzy sliding mode controller design for maximum power point tracking control of a solar energy system. *Trans Institut Meas Control*. 2012;34(5):557-565. doi:10.1177/0142331211407959
21. Al-Majidi SD, Abbod MF, Al-Raweshidy HS. A novel maximum power point tracking technique based on fuzzy logic for photovoltaic systems. *Int J Hydrogen Energy*. 2018;43(31):14158-14171. doi:10.1016/j.ijhydene.2018.06.002
22. Palaniswamy AM, Srinivasan K. Takagi-Sugeno fuzzy approach for power optimization in standalone photovoltaic systems. *Solar Energy*. 2016;139:213-220. doi:10.1016/j.solener.2016.09.027
23. Guenounou O, Dahhou B, Chabour F. Adaptive fuzzy controller based MPPT for photovoltaic systems. *Energ Conver Manage*. 2014;78:843-850. doi:10.1016/j.enconman.2013.07.093
24. Altin N. The type-2 fuzzy logic controller-based maximum power point tracking algorithm and the quadratic boost converter for PV system. *J Electron Mater*. 2018;47(8):4475-4485. doi:10.1007/s11664-018-6312-8
25. Lopez-Guede JM, Ramos-Hernanz J, Altin N, Ozdemir S, Kurt E, Azkune G. Neural modeling of fuzzy controllers for maximum power point tracking in photovoltaic energy systems. *J Electron Mater*. 2018;47(8):4519-4532. doi:10.1007/s11664-018-6407-2
26. Kececioglu OF. Robust control of high gain DC-DC converter using type-2 fuzzy neural network controller for MPPT. *J Intell Fuzzy Syst*. 2019;37(1):941-951. doi:10.3233/JIFS-181770
27. Elobaid LM, Abdelsalam AK, Zakzouk EE. Artificial neural network-based photovoltaic maximum power point tracking techniques: a survey. *IET Renew Power Gener*. 2015;9(8):1043-1063. doi:10.1049/iet-rpg.2014.0359
28. Liu YH, Liu CL, Huang JW, Chen JH. Neural-network-based maximum power point tracking methods for photovoltaic systems operating under fast changing environments. *Solar Energy*. 2013;89:42-53. doi:10.1016/j.solener.2012.11.017
29. Zadeh LA. The concept of a linguistic variable and its application to approximate reasoning—I. *Inform Sci*. 1975;8(3):199-249. doi:10.1016/0020-0255(75)90036-5
30. Ghoddami H, Yazdani A. A single-stage three-phase photovoltaic system with enhanced maximum power point tracking capability and increased power rating. *IEEE Trans Power Deliv*. 2010;26(2):1017-1029. doi:10.1109/TPWRD.2010.2055896
31. Schofield DMK, Foster MP, Stone DA. Low-cost solar emulator for evaluation of maximum power point tracking methods. *Electron Lett*. 2011;47(3):208-209. doi:10.1049/el.2010.2930
32. Andrejašič T, Jankovec M, Topič M. Comparison of direct maximum power point tracking algorithms using EN 50530 dynamic test procedure. *IET Renew Power Gener*. 2011;5(4):281-286. doi:10.1049/iet-rpg.2010.0175
33. Ji YH, Jung DY, Kim JG, Kim JH, Lee TW, Won CY. A real maximum power point tracking method for mismatching compensation in PV array under partially shaded conditions. *IEEE Trans Power Electron*. 2010;26(4):1001-1009. doi:10.1109/TPEL.2010.2089537
34. Piegari L, Rizzo R. Adaptive perturb and observe algorithm for photovoltaic maximum power point tracking. *IET Renew Power Gener*. 2010;4(4):317-328. doi:10.1049/iet-rpg.2009.0006
35. Locment F, Sechilariu M, Houssamo I. Energy efficiency experimental tests comparison of P&O algorithm for PV power system. In: *Proceedings of 14th International Power Electronics and Motion Control Conference EPE-PEMC 2010*. IEEE; 2010:T12-T89.
36. Xiao W, Dunford WG. Evaluating maximum power point tracking performance by using artificial lights. In: *30th Annual Conference of IEEE Industrial Electronics Society, 2004. IECON 2004*. Vol.3. IEEE; 2004:2883-2887.
37. Miyatake M, Veerachary M, Toriumi F, Fujii N, Ko H. Maximum power point tracking of multiple photovoltaic arrays: a PSO approach. *IEEE Trans Aerosp Electron Syst*. 2011;47(1):367-380. doi:10.1109/TAES.2011.5705681
38. Nguyen TL, Low KS. A global maximum power point tracking scheme employing DIRECT search algorithm for photovoltaic systems. *IEEE Trans Ind Electron*. 2010;57(10):3456-3467. doi:10.1109/TIE.2009.2039450

1097007x, 2022, 11, Downloaded from https://onlinelibrary.wiley.com/doi/10.1002/cta.3374 by Kayseri University, Wiley Online Library on [02/01/2024]. See the Terms and Conditions (https://onlinelibrary.wiley.com/terms-and-conditions) on Wiley Online Library for rules of use; OA articles are governed by the applicable Creative Commons License

39. Chen LR, Tsai CH, Lin YL, Lai YS. A biological swarm chasing algorithm for tracking the PV maximum power point. *IEEE Trans Energy Convers*. 2010;25(2):484-493. doi:10.1109/TEC.2009.2038067
40. Xiao W, Zeineldin HH, Zhang P. Statistic and parallel testing procedure for evaluating maximum power point tracking algorithms of photovoltaic power systems. *IEEE J Photovolt*. 2013;3(3):1062-1069. doi:10.1109/JPHOTOV.2013.2257922
41. Zimmermann U, Edoff M. A maximum power point tracker for long-term logging of PV module performance. *IEEE J Photovolt*. 2011; 2(1):47-55. doi:10.1109/JPHOTOV.2011.2174031
42. Li X, Wang Q, Wen H, Xiao W. Comprehensive studies on operational principles for maximum power point tracking in photovoltaic systems. *IEEE Access*. 2019;7:121407-121420. doi:10.1109/ACCESS.2019.2937100
43. Li X, Wen H, Hu Y, Du Y, Yang Y. A comparative study on photovoltaic MPPT algorithms under EN50530 dynamic test procedure. *IEEE Trans Power Electron*. 2020;36(4):4153-4168. doi:10.1109/TPEL.2020.3024211
44. Khater AA, El-Nagar AM, El-Bardini M, El-Rabaie NM. Online learning of an interval type-2 TSK fuzzy logic controller for nonlinear systems. *J Franklin Inst*. 2019;356(16):9254-9285. doi:10.1016/j.jfranklin.2019.08.031
45. El-Nagar AM. Practical implementation for stable adaptive interval A2-C0 type-2 TSK fuzzy controller. *Soft Comput*. 2019;23(19): 9585-9603. doi:10.1007/s00500-018-3523-0
46. Mendel JM. *Uncertain Rule-Based Fuzzy Logic Systems: Introduction and New Directions*. Prentice-Hall; 2001:66-69.
47. Mendel JM. Type-2 fuzzy sets and systems: an overview. *IEEE Computat Intell Mag*. 2007;2(1):20-29. doi:10.1109/MCI.2007.380672
48. Kececioglu OF. Design of type-2 fuzzy logic controller optimized with firefly algorithm for maximum power point tracking of photovoltaic system based on super lift Luo converter. *Int J Numer Model: Electron Netw Devices Fields*. 2022;35(4):e2994. doi:10.1002/jnm.2994
49. Gani A, Kececioglu OF, Kilic E. Dynamic performance evaluation of PI and interval type-2 Takagi-Sugeno-Kang fuzzy controller on positive output Luo converter. *Natural Eng Sci*. 2019;4(3):32-39.
50. Biglarbegian M, Melek WW, Mendel JM. On the stability of interval type-2 TSK fuzzy logic control systems. *IEEE Trans Syst Man Cybern B Cybern*. 2009;40(3):798-818. doi:10.1109/TSMCB.2009.2029986
51. Diaz Martinez D, Trujillo Codorniu R, Giral R, Vazquez Seisdedos L. Evaluation of particle swarm optimization techniques applied to maximum power point tracking in photovoltaic systems. *Int J Circuit Theory Appl*. 2021;49(7):1849-1867. doi:10.1002/cta.2978
52. Motamarri R, Bhookya N, Chitti Babu B. Modified grey wolf optimization for global maximum power point tracking under partial shading conditions in photovoltaic system. *Int J Circuit Theory Appl*. 2021;49(7):1884-1901. doi:10.1002/cta.3018
53. Kumari N, Kumar SS, Laxmi V. Design of an efficient bipolar converter with fast MPPT algorithm for DC nanogrid application. *Int J Circuit Theory Appl*. 2021;49(9):2812-2839. doi:10.1002/cta.3020

How to cite this article: Gani A, Sekkeli M. Experimental evaluation of type-2 fuzzy logic controller adapted to real environmental conditions for maximum power point tracking of solar energy systems. *Int J Circ Theor Appl*. 2022;50(11):4131-4145. doi:10.1002/cta.3374

1097007x, 2022, 11, Downloaded from https://onlinelibrary.wiley.com/doi/10.1002/cta.3374 by Kayseri University, Wiley Online Library on [02/01/2024]. See the Terms and Conditions (https://onlinelibrary.wiley.com/terms-and-conditions) on Wiley Online Library for rules of use; OA articles are governed by the applicable Creative Commons License